Nanoreactors by Programmed Enzyme Encapsulation Inside the Capsid of the Bacteriophage P22

Dustin P. Patterson,[†,‡] Peter E. Prevelige,[§] and Trevor Douglas[†,‡,*]

[†]Department of Chemistry and Biochemistry, [‡]Center for Bio-Inspired Nanomaterials, Montana State University, Bozeman, Montana 59717, United States, and [§]Department of Microbiology, University of Alabama, Birmingham, Alabama 35294, United States

ABSTRACT

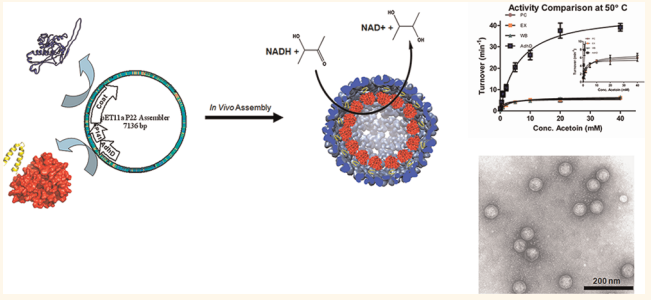

The virus like particle (VLP) derived from bacteriophage P22 presents a unique platform for constructing catalytically functional nanomaterials by encapsulation of enzymes into its interior. Encapsulation has been engineered to be genetically programmed allowing "one pot" synthesis and incorporation of desired enzymes. The unique characteristic that separates P22 from other VLP systems is the ability to modulate the overall volume and porosity of the VLP structure, thus controlling substrate access to the encapsulated enzyme. The present study demonstrates incorporation of an enzyme, alcohol dehydrogenase D, with the highest internal loading for an active enzyme by any VLP described thus far. In addition, we show that not only does encapsulating AdhD inside P22 affect its kinetic parameters in comparison with the "free" enzyme, but transformation of P22 to different morphological states, which changes the internal volume of the VLP, yields changes in the overall activity of the encapsulated enzyme as well. The findings reported here clearly illustrate that P22 holds potential for synthetic approaches to create nanoreactors, by design, using the power of highly evolved enzymes for chemical transformations.

KEYWORDS: encapsulation · enzymes · enzyme catalysis · nanocontainers · virus-like particles

The study of biomimetic materials has emerged as an important field where inspiration and raw materials from biology can be synergized with synthetic approaches to achieve new designer materials that are functional at many length scales. The ability by which nature is able to organize macromolecules, for example protein subunits, into precisely defined multisubunit structures, often with multiple functions, is unparalleled in the synthetic world. When combined with the ability to catalyze precise chemical transformations, as observed in enzymes, there is the potential for creating new dynamic materials with tunable reactivity. Researchers have investigated coupling enzymes to both synthetic and biological platforms, such as linking enzymes to immobile substrates, including porous materials,[1−3] encapsulation inside lipid and polymeric vesicles,[4−8] and encapsulation into virus-like particles (VLPs)[9−12] to mimic cellular compartmentalization and localization of enzymes, which, in many cases, resulted in modulated enzyme activities. Encapsulation of enzymes into nanostructures has the potential to create "nanoreactors" with unique properties such as, for example, enhanced activities, ability to conjugate the multienzyme structure to surfaces, protection against enzyme degradation, and resistance of enzyme denaturation in organic solvents. Use of lipid and polymeric vesicles present significant downsides for use in creating nanoreactors as they can suffer poor stability, often form structures of varying sizes, and their membranes often exhibit low permeability to substrates.[5,9,13] VLPs on the other hand possess properties that overcome many of these issues and the ability to use biology to synthesize all the building blocks (both VLP and enzyme) and direct their self-assembly, make them attractive candidates for constructing protein nanoreactors, using a genetically programmed approach.

Virus-like particles (VLPs) are a class of multimeric proteins derived from virus capsids, which form symmetric protein shells that define a hollow interior space. VLPs, and other protein cage-like architectures, have been well studied as hosts for encapsulation of an array of guest species,[9−12,14−42] including examples of active enzyme encapsulation.[9−12] The regular discrete size,

* Address correspondence to tdouglas@chemistry.montana.edu.

Received for review February 6, 2012 and accepted May 24, 2012.

Published online May 24, 2012
10.1021/nn300545z

© 2012 American Chemical Society

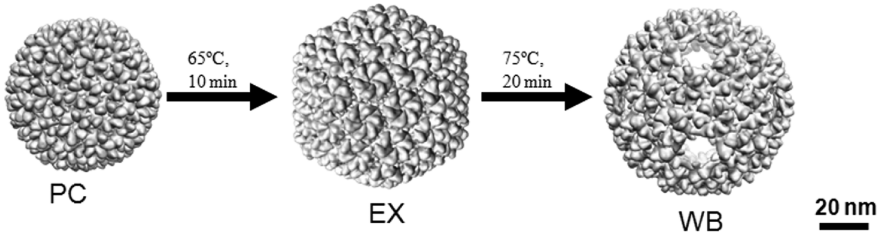

Figure 1. Display of the three different morphologies that P22 can adopt.[69] The P22 VLP is produced as a procapsid structure (PC), which can be transformed to either an expanded shell form (EX) or "wiffleball" form (WB) depending on heating conditions. For simplicity, transformation to WB is shown from the EX form although WB can be obtained from PC directly using the same heating conditions as displayed for going from EX to WB.

high stability, and substrate permeability through channels in the protein shell of VLPs provide a distinct advantage over other methods for encapsulation. Observations that nature also uses proteins to construct nanocompartments for encapsulating proteins and enzymes provide further inspiration for using VLPs for enzyme encapsulation.[43−48] Incorporation of enzymes or other proteins into the interior of VLPs has been performed either by *in vitro* packaging through disassembly and reassembly of VLPs in the presence of protein cargo or through genetic fusion of protein cargo to components that direct localization into the particle interior. To date relatively few examples of enzyme encapsulation inside VLPs have been described.[9−12] Studies performed thus far have utilized small viral capsids ($T = 3$) with limited loading capacity (a maximum of 18 enzymes per capsid has been reported[10]). In addition, systems described thus far require the conditions for modifying the internal enzyme concentration be determined empirically by either modification of protein expression conditions to lower or increase the number of enzymes that are encapsulated[10] or for nonspecific *in vitro* incorporation by determining the concentration ratio of protein mixed with capsid to give the altered concentration.[9,12] Until now, no VLP enzyme encapsulation system has been described that allows modulation of VLP porosity or capsid volume, which allow for the controlled adjustment of the catalytic properties of the nanoreactor.

In this study we have utilized an encapsulation system derived from the *Salmonella typhimurium* bacteriophage P22 capsid. This VLP is composed of 420 copies of a 46.6 kDa coat protein (CP) that assembles into a $T = 7$ icosahedral capsid with the aid of approximately 100−330 copies of a 33.6 kDa scaffolding protein (SP).[49] The SPs are incorporated on the interior of the capsid through noncovalent association of the coat and C-terminus of the SPs, which direct the assembly of the capsid *via* a head-full mechanism. In addition, the P22 VLP undergoes a series of characterized structural transitions upon heating, which yields large changes in internal volume and external accessibility to its hollow interior through dramatic changes in capsid porosity. Heterologous expression of P22 CP together with SP results in self-assembly of the compact procapsid (PC) structure, which has an external diameter of 58 nm. Gentle heating at 65 °C for 10 min causes irreversible expansion of the PC structure yielding a 64 nm P22 structure referred to as the expanded form (EX) together with loss of the SP.[50,51] The resulting change in diameter from PC to EX morphology results in a near doubling of the effective volume of the internal cavity (58 000 nm^3 in PC to 113 000 nm^3 in EX). An additional transformation can be induced by heating either PC or EX P22 at 75 °C for 20 min (or more), which causes selective release of subunits from the 12 5-fold icosahedral vertices, yielding a structure containing large 10 nm holes at each of the 5-fold vertices known as "wiffleball" (WB) structure.[50,52] There is no significant difference in diameter between EX and WB P22,[50,52] but the presence of the 10 nm holes in the WB structure allows far greater molecular access between the interior of the VLP and the bulk solution. From structural studies both the PC and EX form have smaller 2 nm pores in the VLP shell between the exterior and interior of the VLP. Figure 1 shows the different morphological forms of P22 with a scheme showing the conditions required for transformation to the different forms.

Previous studies have shown that the SP of P22 interacts with the CP only through the last few C-terminal residues and the full length protein can be highly modified at the N-terminus while still maintaining the ability to guide the assembly of CP into the native-like P22 capsid structure.[53,54] These modifications can include either the deletion of large numbers of amino acids from the N-terminus or the fusion of another gene product to the truncated SP. Truncated SPs have been exploited as a vehicle for the programmed *in vivo* incorporation of proteins and peptides to the interior of the P22 VLP. We have previously shown that cargo proteins, specifically fluorescent proteins (FP), expressed as SP fusions are incorporated into the interior of P22 VLPs when heterologously expressed in *E. coli* together with CP.[21] Using this SP fusion strategy, FPs were incorporated in high copy number, with up to 300 FP per VLP observed. In addition, incorporation of FP-SP fusion to the interior did not alter the VLPs ability to undergo transitions to the EX or WB and also showed that FP was unable to escape from the EX form,

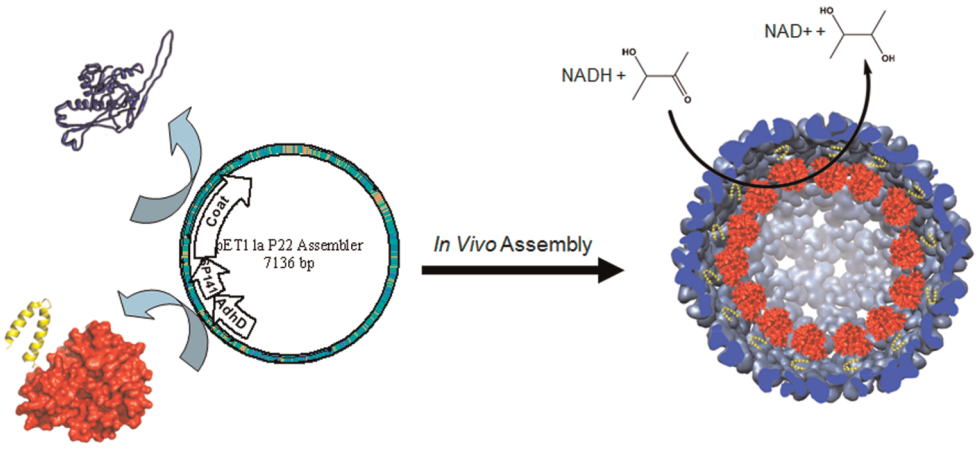

Figure 2. Schematic representation of *in vivo* recombinant expression and encapsulation of an AdhD-SP fusion inside of the assembled P22 capsid and the reaction catalyzed by the encapsulated enzyme. The assembly of the capsid from coat protein (blue) and the AdhD-SP fusion (red) is directed by the C-terminus of the truncated scaffold (yellow).

although the unstructured SP could access the exterior through the 2 nm pores of P22 and be cleaved from FP by thrombin at a specifically engineered site.[21] However, upon transformation to WB, FP was able to escape the internal confines of P22 through the 10 nm holes of WB due to the smaller diameter of FP compared to the pores. Proteins with larger diameters are expected to be retained within the WB structure and this highlights the utility of P22 as a novel system for incorporating enzymes to build dynamic protein nanoreactors. P22 is an intriguing encapsulation system whose volume can be systematically modulated through the PC → EX morphological transformation, which may have significant effects on activity due to differences in crowding and confinement. In addition, the transition from EX (or PC) to WB can be used to allow greater substrate access to the encapsulated enzymes—a unique feature of the P22 system. In addition to these unique qualities of P22, we and others have shown that VLPs can be immobilized to surfaces and patterned in a specific manner,[55−58] which is potentially useful toward practical future applications using VLPs encapsidating enzymes.

As a first step toward making an enzyme an encapsulated nanoreactor using the P22 assembly system, we utilized the enzyme alcohol dehydrogenase D (AdhD) from the hyperthermophile *Pyrococcus furiosus*. AdhD is a 32 kDa monomeric protein that catalyzes ketone/alcohol reduction−oxidation and can be easily assayed by following loss of NADH upon reduction of ketone substrates.[59] A schematic model of the envisioned AdhD-P22 nanoreactor assembly and catalysis is provided in Figure 2. Alcohol dehydrogenases present useful industrial biocatalysts of considerable interest in the food, pharmaceutical, and fine chemical industries.[59] The thermostability of AdhD allows us to exploit the structural transformations of the P22 VLP to different morphological states without thermally damaging the enzyme. In addition, it has been previously shown that fusion of peptides to either the N- or C-terminus of AdhD does not destroy activity,[60] which suggests that making a fusion of SP and AdhD will not hamper proper folding of AdhD. Our results show that P22 can be used to encapsulate active enzymes and encapsulation modulates kinetics parameters in comparison with "free" enzyme.

RESULTS AND DISCUSSION

The gene encoding AdhD was amplified from genomic *P. furiosus* and inserted into the pET11 P22 assembler vector, previously described,[21] so that expression would yield AdhD fused at the N-terminus of the truncated SP_{141} (Supporting Information). Expression from the vector in *E. coli* (BL21(DE3)) yielded P22 VLPs, with encapsulated AdhD, that were indistinguishable from wild type P22. SDS-PAGE showed the encapsulated AdhD migrated at approximately 50 kDa (Figure 3A.1), the expected size for the AdhD-SP fusion (50.7 kDa). Native agarose gel shift assays showed that the procapsid (PC) containing AdhD could be transformed to either the expanded (EX) or wiffle ball (WB) morphology by heating to 65 or 75 °C, respectively, although the efficiency of transformation to EX was limited to about 50% (Figure 3A.2). TEM images further verified that the packaging did not noticeably alter the P22 structure and corroborated the native agarose gel shift data for transformation. TEM images of PC and WB samples showed particles with an average diameter of 54.4 ± 1.92 and 60.7 ± 2.19, while EX showed two size distributions of 54.3 ± 0.95 and 60.2 ± 1.79 at approximately 1:1 ratio (46 and 54%, respectively). TEM images also revealed evidence for dense packing of protein on the interior of P22 (Figure 3B).

To determine the average amount of AdhD encapsulated per capsid, and further characterize changes that occur upon going from PC to EX and WB, we utilized HPLC size exclusion chromatography coupled to multiangle light scattering (MALS) and refractive

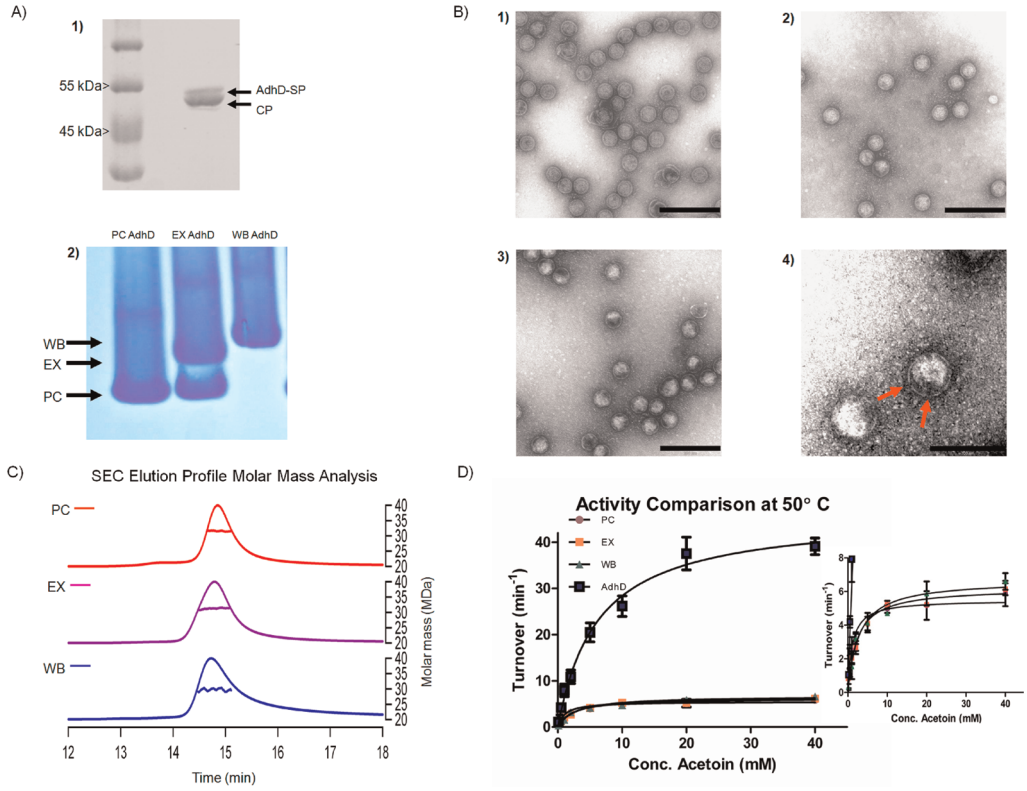

Figure 3. Characterization of P22 encapsidated AdhD. (A) (1) SDS-PAGE gel of the purified AdhD-SP P22 showing AdhD-SP (upper arrow, expected 50 kDa) and CP (lower arrow, expected 46.6 kDa). (2) Agarose gel shift assay of AdhD-SP P22 with lanes labeled according to their sample identity. (B) Transmission electron micrographs of different morphologies of AdhD-SP P22: (1) procapsid (PC); (2) expanded shell (EX); (3) wiffle ball (WB); and (4) higher magnification of wiffle ball form with large pores visible (red arrows). Scale bars for images 1−3 are 200 nm and image 4 is 100 nm. (C) Plots of the size exclusion chromatography profiles and molecular weight analysis (from MALS) of procapsid (red trace), expanded shell (purple trace), and wiffle ball (blue trace) AdhD-SP P22. (D) Plots of results for substrate activity assays of "free" and encapsidated AdhD taken at 50 °C.

index (RI) detectors. Analysis of the MALS/RI data (Figure 3C) showed a molecular weight for the AdhD-SP P22 PC of 32.3 ± 0.65 MDa, compared to that of empty P22 (no scaffold), which had a M_w of 19.1 ± 0.05 MDa (as compared to the expected M_w of ~19.7 MDa). The difference in M_w of 12.6 MDa from the theoretical M_w of empty capsid corresponds to a loading of 249 ± 13 AdhD enzymes per capsid (see Supporting Information of detailed description for calculating the number of AdhD enzymes per capsid). Transformation to EX did not change the overall mass (32.5 ± 1.3 MDa) from that observed for PC, although the elution profile showed a shorter retention time of EX and an increase in the radius of gyration from 21.8 to 22.5 nm. It is important to note that radius values determined by MALS are the radius of gyration, which are dependent not only on the radius of the particle but also the mass distribution of the particle, explaining the smaller radius values observed for the enzyme-filled P22 from those expected from structural studies of P22 (see Supporting Information). Further heating of the AdhD-SP P22 to 75 °C, to form the WB structure, yielded a M_w of 29.4 ± 0.29 MDa. This loss of 2.9 MDa is consistent with the expected mass loss from removal of subunits at the 12 5-fold vertices (Δ of 2.8 MDa expected), which was also confirmed by TEM (Figure 3B), but without loss of the cargo protein. The observation that little or no AdhD protein was lost from WB P22 provides evidence that AdhD has an overall diameter larger than the 10 nm holes in WB, as smaller proteins like FP have been observed to freely diffuse out of the interior of WB P22.[21] In addition, WB had a slightly larger radius (22.9 nm) than the 65 °C expanded sample, consistent with this sample being a nearly 1:1 mixture of EX and PC as observed in the native gel electrophoresis and TEM investigations. The transformation to the WB structure however was quantitative as measured by native gel electrophoresis with no evidence of residual PC or EX forms. The number of enzymes per capsid found by MALS was further supported by SDS-PAGE densitometry analysis (see Supporting Information), which gave a ratio of CP to AdhD-SP corresponding to 235 enzymes per capsid.

The number of AdhDs encapsulated in P22 represents the largest number of enzymes synthetically encapsulated by a VLP reported thus far and is achieved through a genetically programmed self-assembly. In addition, the packaging of ~250 AdhDs into the P22

TABLE 1. Kinetic Results for Encapsidated and Free AdhD for the Catalysed Reaction Using Acetoin as the Substrate, NADH as the Cofactor[a]

Sample	k_{cat} (sec^{-1})	$K_{M,Ace,App}$ (mM)	$K_{M,NADH,App}$ (μM)	$k_{cat}/K_{M,Ace,App}$ (sec^{-1} mM^{-1})
		50 °C		
PC	0.097 ± 0.005*	1.23 ± 0.31**	64.8 ± 10.3	0.079
EX	0.104 ± 0.004*	2.50 ± 0.39*	44.2 ± 13.1	0.045
WB	0.114 ± 0.004*	2.93 ± 0.43**	48.6 ± 12.7	0.039
AdhD	0.770 ± 0.031*	6.23 ± 0.87*	22.6 ± 4.31	0.124
		60 °C		
EX	0.336 ± 0.014*	5.61 ± 0.88*	75.7 ± 13.2	0.060
WB	0.369 ± 0.018*	7.00 ± 1.18	53.1 ± 10.9	0.053
AdhD	2.01 ± 0.081*	9.26 ± 1.22*	52.1 ± 9.82	0.217
		70 °C		
WB	0.787 ± 0.052*	13.2 ± 2.59	143 ± 16.1	0.060
AdhD	4.23 ± 0.280*	20.8 ± 3.65	39.2 ± 6.62	0.204

[a] Kinetic parameters marked with a single asterisk (*) denote statistically significant ($P \leq 0.05$) differences in values in comparison to the "free" AdhD. Kinetic values marked with an additional asterisk (*i.e.* **) indicate encapsidated samples that have statistically different values in comparison with each other (*i.e.*, PC *vs* WB).

gives a local concentration, or confinement molarity (M_{conf}), of 7.16 mM AdhD, which far exceeds the maximum M_{conf} of 1 mM previously described in the literature.[9] On the basis of the volume of the PC cavity and the estimated volume of the folded AdhD protein, the packaging of 250 AdhD proteins results in an occupancy of ~27% of the available volume (see Supporting Information). This is approximately one-third of the occupancy attainable by a random close packing model (64%).[61] In the absence of additional engineered AdhD self-interactions, higher density occupancy of AdhD within the capsid is not expected since full length SP, a smaller protein than AdhD, is only able reach 330 copes per VLP, corresponding to a similar occupancy density within the capsid.[49] Furthermore, expansion of AdhD-SP P22 PC to either EX or WB results in an approximate doubling of internal volume of the capsid, producing a M_{conf} that drops to 3.2 mM, but which still exceeds the M_{conf} of other systems. Activity assays were performed at 50, 60, and 70 °C, omitting AdhD-SP P22 forms from temperatures that would cause transformation to the other P22 morphologies (*i.e.*, PC activity was not measured at 70 °C because it would transform into the WB form at that temperature). Results from the assays showed that encapsulated AdhD followed Michaelis–Menten kinetics, and the kinetic parameters determined for each data set are displayed in Table 1. Data for "Free" AdhD at 50 °C showed substrate inhibition at concentrations above 40 mM acetoin (3-hydroxybutan-2-one), which was not observed for encapsulated AdhD (see Supporting Information). Therefore data fitting for "free" AdhD using a Michaelis–Menten model was performed using up to 40 mM substrate concentration, although fits using a substrate inhibition model yielded similar results (see Supporting Information). An overlay of the fitted data for PC, EX, WB, and "free" AdhD at 50 °C is shown in Figure 3D, and all other data plots are provided in the Supporting Information. No statistically relevant difference in kinetic parameters was observed between "free" AdhD and "free" AdhD mixed with empty P22, and only "free" AdhD will be discussed further (see Supporting Information for comparison).

Inspection of the kinetic parameters reveals that encapsulation of AdhD significantly lowers the k_{cat} (activity, units of sec^{-1}) relative to the free enzyme at all temperatures by about 7-fold. Reduction in enzyme activity has previously been observed in experiments using crowding agents, although depending on the enzyme system there are also reports of increases in activity with crowding.[62,63] Rate declines have been attributed to constraints on conformation change during catalysis, diffusion of product from enzyme–substrate complex, and to changes in the ratio of activity coefficients between native enzyme and an enzyme–substrate complex.[62,63] Another explanation for the reduced rate is the possibility that not all the encapsulated enzymes are active. While we know the "free" AdhD-SP fusion does not appear to have any apparent problems that affect activity we cannot specifically rule out the possibility that the percentage of active enzymes is lower upon encapsulation. However, this is a fundamental and general problem in enzymology since damaged or unreactive enzymes in any sample preparation is neglected. Assessment of this, even using single molecule enzyme assays, is hard to address since inactive enzymes are not observable. Our analysis is thus in accordance with the practice common to traditional enzymology as both encapsulated and free AdhD have the same potential for enzyme inactivation. Our findings that encapsulation of AdhD decreases the overall activity of the enzyme agrees with trends observed for the few examples of VLP encapsulation of enzymes described previously, discussed in more detail below. "Free" AdhD k_{cat} values found in our study are in good agreement, within error, for those found by Wheeldon *et al*. who found values of 0.8 ± 0.2 s^{-1} and ~1.8 ± 0.8 s^{-1} for fusion proteins of AdhD at 45 and 60 °C respectively.[60] A k_{cat} value of 11.7 s^{-1} was found by Machielson et al. at 70 °C, almost 3-fold higher than found in our results.[59] The differences in our value may arise from, in addition to differences in experimental conditions and technique, the fact that our "free" AdhD was expressed as a fusion protein with P22 scaffold protein, and Wheeldon *et al*. found that a fusion protein of AdhD showed modified kinetics from the wild type AdhD used by Machielson et al.[59,60]

Significant differences were also observed for the apparent Michaelis–Menten constants of the acetoin substrate ($K_{M,Ace,App}$) for "free" AdhD and encapsulated

AdhD. In all cases, the $K_{M,Ace,App}$ of AdhD was lowered upon confinement irrespective of temperature and the morphological state of P22 and these differences were found to be statistically significant ($P \leq 0.05$). The $K_{M,Ace,App}$ for the encapsulated AdhD in the PC was observed to be 1.23 ± 0.31 mM, whereas expansion to EX and WB resulted in $K_{M,Ace,App}$ of 2.50 ± 0.39 mM and 2.93 ± 0.43 mM, respectively. This more than 2-fold increase in $K_{M,Ace,App}$ coincides with an approximate 2-fold increase in internal volume of the VLP for the samples assayed at 50 °C. Comparison of the encapsidated AdhD with the "free" AdhD form showed a $K_{M,Ace,App}$ 5-fold lower for AdhD-P22 PC and 2-fold lower for both AdhD-P22 EX and WB in comparison with the "free" AdhD enzyme for measurements made at 50 °C. The results found at 50 °C show a consistent trend of a decrease in $K_{M,Ace,App}$ upon greater M_{conf}, which is also observed for the data measured at 60 and 70 °C (see table). Values for $K_{M,Ace}$ have only been reported for wild type AdhD at 70 °C, which was found to have a much lower value (6.5 mM) than was found for our fusion AdhD. Decreases in K_M of up to 4-fold have also been observed in systems using macromolecular crowding agents, which have been primarily suggested to result from change in enzyme conformation. Interestingly, although the decrease in $K_{M,Ace,App}$ is observed upon confinement, the difference between the $K_{M,Ace,App}$ of encapsidated and "free" AdhD becomes smaller with increases in temperature (to the point where there is no statistical difference). One possible explanation for this observation is that increasing temperature causes a structural rearrangement of the AdhD structure producing a binding pocket conformation for Acetoin more like that of "free" AdhD, although overall mechanical properties important for catalysis are still inhibited and a greater change in rate is not also observed.

The apparent Michaelis–Menten constants observed for the NADH cofactor, $K_{M,NADH,App}$, showed a different effect from that of the substrate. There appeared to be a general trend that encapsidation increases the $K_{M,NADH,App}$ of AdhD, although the overall difference and statistical significance vary, particularly at the two lower temperatures. For the data at 50 °C the PC AdhD was found to have a 2-fold higher $K_{M,NADH,App}$ than the "free" AdhD, with the other P22 forms showing $K_{M,NADH,App}$ values intermediate between that of "free" and PC AdhD. The data at 60 °C showed no difference in $K_{M,NADH,App}$ between WB and "free" AdhD, with a nonstatistically significant increase for EX AdhD $K_{M,NADH,App}$. However, at 70 °C an approximate 4-fold increase in the WB AdhD $K_{M,NADH,App}$ to that of "free" AdhD was found. It is not immediately apparent why there is a large difference for $K_{M,NADH,App}$ at 70 °C, but little or no difference at the lower temperatures. It has been previously suggested that such effects could be due to the lower diffusion rates of the VLP-enzyme capsule;[10] however, it is difficult to draw that parallel here since the change is not the same over all temperatures. Values for $K_{M,NADH}$ have only been reported for wild type AdhD at 70 °C, which was found to have a much lower value of 97 μM, which is slightly higher than the $K_{M,NADH,App}$ found for our fusion AdhD.

One of the more intriguing results from this study is that the kinetic parameters found for EX and WB AdhD are nearly the same. The slight differences can be attributed to the fact that all of the PC form was not transformed to EX and so the EX sample still contained some PC form resulting in observed kinetics values intermediate between that of the PC and WB values. In the P22 system the transformation from PC (or EX) to WB is expected to dramatically change substrate molecular access to the interior of the capsid due to the formation of large 10 nm holes in the VLP structure. EX and WB have approximately the same volume, and the observation that there is no difference in their kinetic parameters provides evidence that the substrate and cofactor diffusion are not impeded by the capsid wall, and the 2 nm pores of P22 in the PC and EX forms, and are sufficient in size to allow free diffusion of substrate and cofactor across the capsid. No evidence for disassembly reassembly has been observed during characterization of P22 (using methods such as size exclusion chromatography and analytical ultracentrifugation) that could potentially allow greater substrate access regardless of the morphological state. Previous experiments of VLP encapsidated enzymes made the assumption that substrates and cofactors were able to freely diffuse through the protein coat by way of similar small pores found in PC and EX P22 constructs, although they were not able to explicitly test the assumption by increasing access to the interior as we have demonstrated here with WB P22. Our findings provide direct evidence that this is the case for these relatively small substrates and cofactors.

The results found for AdhD encapsidation, that both k_{cat} and $K_{M,Ace,App}$ decrease upon greater packing and thus increased crowding, parallels results observed for two different enzymes using conventional crowding agents. Assays performed by Olson on hexokinase using BSA as a crowding reagent and isothermal titration calorimetry measurements found reduction in both k_{cat} and K_M of 30% and no change in the overall catalytic efficiency (k_{cat}/K_M).[64] They proposed that these changes resulted from change in the ratio of activity coefficients between the native enzyme and enzyme–substrate complex. Interestingly, our results also show that the overall catalytic efficiency of PC AdhD achieves nearly the same catalytic efficiency as that of "free" AdhD, suggesting that our system may follow a similar model or that this is a unique regulatory mechanism for AdhD. In a different study, by Jiang and Guo, on isochorismate synthase, they found the

decline in both k_{cat} and K_M resulted from changes in structure.[65] Conformational changes have been typically used to explain the kinetic changes that occur in crowding experiments and may be at play in our encapsidated AdhD.[62] We are not implying that the results from these studies are the definitive reason for the results observed for AdhD since different enzymes function through different mechanistic and structural dynamics. These studies present viable explanations given the limited data available in the literature looking at this type of confinement and crowding, with no reports available for crowding studies of AdhD or similarly related alcohol dehydrogenases. Pressure studies have been reported for alcohol dehydrogenase from yeast, however these studies looked at the oxidation of the alcohol, the reverse reaction of what we characterized, and additionally looked at volume based kinetics parameters that are not comparable with the results described here.[66−68]

Our results for encapsidation of AdhD agree well with results from enzyme encapsulation studies performed using different VLP systems. Encapsulation of N-terminal aspartate dipeptidase peptidase E in Qβ reduced the activity by more than half compared to the free enzyme[10] and slightly lower rates of enzymatic activity were observed for SV40 encapsulated cytosine deaminase.[11] In addition, the study of encapsulated firefly luciferase in Qβ showed that as the M_{conf} increased a drop in activity of nearly half compared to the free enzyme was reported.[10] Studies by Cornelissen and co-workers, pioneers in enzyme-VLP encapsulation studies, on encapsulation of *Pseudozyma antartica* lipase B (PalB) in Cowpea chlorotic mottle virus (CCMV) showed an increase in activity over free enzyme, but the rate was observed to decrease as the number of enzymes encapsulated was increased.[9] The highest M_{conf} assayed for PalB in the CCMV study was 1 mM, more than 7-fold and three and a half-fold lower than the M_{conf} found for AdhD-SP P22 in PC, EX, and WB forms, respectively. These results suggest that confinement and crowding overall lowers the activity of enzymes, however the VLPs used in other studies have been limited in their ability to reach M_{conf} high enough to probe the full range of effects we have observed and reported here for AdhD encapsulation in P22.

CONCLUSION

The results from our study show that P22 is a novel and viable VLP for creating designer nanoreactors encapsulating an enzyme cargo of choice and for studying enzyme crowding effects. The *in vivo* genetically programmed packaging and assembly observed for the P22 system presents an efficient "one-pot" expression-assembly system that provides specific directed packaging of protein cargo and eliminates assembly problems associated with *in vitro* assembly strategies. In addition, we have shown that P22 can undergo dynamic structural changes that increase the overall volume and substrate access, a unique quality that is not found in any other VLP system described thus far. The larger size of P22 allowed internal packaging (M_{conf}) of AdhD in excess of 7 mM, the highest found in the literature thus far, or ~300 g/L, which nears the level found for proteins in cellular environments. We found that encapsulation of AdhD in P22 did not produce a more active enzyme, which was not necessarily the primary objective. We observed that encapsulation was able to reverse substrate inhibition seen for free enzyme and the overall catalytic efficiency was maintained (for PC), both of which are positive attributes that provide a unique advantage over the "free" enzyme. In addition, we have previously shown that protein cages can be immobilized to surfaces and patterned in specific arrays, which could be done with P22 encapsulating enzymes to produce enzyme active surfaces for use in flow cells or other devices where binding enzyme to surfaces in a patterned or specific manner is required. Often immobilizing free enzymes to surfaces causes complete loss of activity, and use of P22 as a carrier could circumvent this problem. Further research to investigate multimeric enzymes, which present dissociation and activity problems when ligated to surfaces, incorporated into the P22 encapsulation system will provide greater support for its use for such applications. In addition, P22 has potential applications for exploring crowding and confinement effects as well as encapsulation of multienzyme complexes to form synthetic metabolons. The findings reported here illustrate that P22 has enormous potential for synthetic approaches to create nanoreactors, by design, using the power of highly evolved enzymes for chemical transformations.

MATERIALS AND METHODS

Materials. DNA modifying enzymes were purchased from New England Biolabs and Promega. DNA primers were purchased from Eurofins MWG Operon (Huntsville, AL). *E. coli* BL21(λDE3) and XL1 electrocompetent cells were purchased from Agilent Technologies. *P. furiosus* DNA was purchased from ATCC. QIAquick gel extraction kit and QIAprep Spin Miniprep kit were purchased from Qiagen (Valencia, CA). Lysozyme, acetoin, and NADH were purchased from Sigma Aldrich. All other chemical reagents were from Fisher Scientific (Pittsburgh, PA).

DNA Molecular Biology. The AdhD gene was amplified from genomic *P. furiosus* DNA using the primers 5′-AAAACATATGGAGCTCATGGCAAAAAGGGTA AATGCATTCAACGA-3′ and 5′-AAAACTCGAGCCATGGCACACACCTCCTTGCCATCT-3′ by PCR using OneTaq (New England Biolabs). The resulting PCR AdhD gene product was digested with SacI and NcoI and ligated into the previously described pET11 P22 assembler plasmid cut with

the same restriction enzymes. The ligation reaction was transformed into XL1 electrocomponent *E.coli*, colonies were screened by restriction enzyme digestion, and all hits were sequenced (Seqwright, Tx) for complete verification. After verifying the correct sequence, DNA was transformed into BL21(λDE3) for expression.

Protein Expression and Purification. *E. coli* strains harboring expression constructs were grown on LB medium at 37 °C in the presence of ampicillin to maintain selection for the plasmid. Expression of the genes were induced by the addition of isopropyl β-D-thiogalactopyranoside (IPTG) to a final concentration of 0.5 mM once the cells reached early log phase (OD_{600} = 0.8). Cultures were grown for 4 h after the addition of IPTG, then the cells were harvested by centrifugation, and cell pellets were stored at −20 °C overnight.

Cell pellets were resuspended in Lysis buffer (50 mM sodium phosphate, 100 mM sodium chloride, pH 7.6) with lysozyme and RNase added and incubated on ice for 30 min. The cell suspension was lysed by sonication. Cell debris was removed by centrifugation at 12000*g* for 45 min at 4 °C. The supernatant was decanted and spun an additional 45 min at 12000*g* to remove any excess cellular debris. P22 was purified from the supernatant by ultracentrifugation over a 35% (w/v) sucrose cushion. The resulting viral pellet was resuspended in PBS (50 mM sodium phosphate, 25 mM sodium chloride, pH 7.0) and then purified over an S-500 Sephadex size exclusion column using a AKTA Pharmacia FLPC. Flow rate for SEC purification was 1 mL/min of PBS. Fractions taken from SEC containing P22 were concentrated by ultracentrifugation and resuspension of the resulting viral pellet in an adequate volume of PBS. Control AdhD-scaffold fusion protein ("free" AdhD) was purified by heating the supernatant after sonication and centrifugal removal of cell debris at 80 °C in a water bath for 30 min to produce a white cloudy precipitate. Precipitated material was removed by centrifugation at 12000*g* for 30 min at 4 °C. "Free" AdhD was further purified by ion exchange chromatography over a Mono Q column. IEC fractions containing AdhD were concentrated and dialyzed against PBS. Concentrations for the P22 construct were determined by UV absorption measured at 280 nm assuming a molar extinction coefficient ε_{280} = 44380 M^{-1} cm^{-1} and ε_{280} = 62990 M^{-1} cm^{-1} (calculated using Protein Calculator v3.3, Chris Putnam, Scripps) for coat and AdhD-SP, respectively, and the ratio of AdhD-Scaffold fusion to Coat determined by densitometry and the molecular weight determined from size exclusion chromatography and for "Free" AdhD the ε_{280} = 56590 M^{-1} cm^{-1} was used, which takes into account loss of the scaffold (near the thrombin site) during IEC purification (see further explanation and an example of the calculation of the concentration of AdhD in the calculations section of the Supporting Information, section 8).

Size Exclusion Chromatography with Multiangle Light Scattering and Refractive Index Detection. Samples were separated over a WTC-0200S (Wyatt Technologies) size exclusion column utilizing an Agilent 1200 HPLC to apply and maintain a 0.7 mL/min flow rate of 50 mM phosphate, pH 7.2 buffer containing 100 mM sodium chloride and 200 ppm sodium azide. Samples of 25 μL were injected onto the column, and the total run time was 30 min. Samples were detected using a UV−vis detector (Agilent), a Wyatt HELEOS multi-angle laser light scattering (MALS) detector, and an Optilab rEX differential refractometer (Wyatt Technology Corporation). The number average molecular weight, Mn, was calculated with Astra 5.3.14 software (Wyatt Technology Corporation) based on the molecular weight distribution.

Transmission Electron Microscopy. Samples (10 μL, 0.1 mg/mL protein) were applied to Formvar coated grids and incubated for 30 s, and excess liquid was wicked away with filter paper. Grids were then washed with 10 μL of distilled water, wicking away liquid shortly after the addition with filter paper, Grids were then stained with 5 μL of 1% uranyl acetate, and excess stain was wicked away with filter paper. Images were taken on a LEO 912AB transmission electron microscope at accelerating voltage of 100 kV.

SDS-PAGE and Densitometry. Protein samples were mixed with 4× loading buffer containing DTT, and heated in a boiling water bath for 10 min, removed, and spun down on a benchtop centrifuge. Samples were run separated on a gel containing a 5% acrylamide stacking gel and a 20% acrylamide running or separating gel using a constant current of 35 mA for approximately 1.5 h. Gels were stained with coomassie blue stain, rinsed with water, and destained. Images were taken on a UVP MultDoc-IT Digital Imaging System and on an Alpha Imager 2200 for densitometry measurements. Images taken on the Alpha Imager 2200 were analyzed using the Alpha Ease FC software to determine the ratio of CP to AdhD-SP fusion protein.

Agarose Gel Shift Assay. Samples were mixed with loading buffer (40% glycerol, bromophenol blue) and subsequently loaded into their respective well. Gel shift assays were run on a 1% agarose gel (w/v) at a constant voltage of 65 V for 3 h. The running buffer was a 40 mM Tris, 5 mM acetate, 1 mM EDTA, pH 8.2 solution. Gels were stained with coomassie blue for 30 min and subsequently rinsed with deionized water and destained. Images were taken on a UVP MultDoc-IT Digital Imaging System.

Dynamic Light Scattering. Samples were spun down at 17000*g* for 10 min and filtered through a 0.2 μm syringe filter prior to taking dynamic light scattering measurements. Measurements were taken at 90° with a 661 nm diode laser (Brookhaven 90Plus particle size analyzer), and the correlation function was fit to a non-negatively constrained least-squares analysis to yield the hydrodynamic radius (R_H) for the particles.

AdhD Kinetics Assays. Activity assays were carried out on a Cary 50 Bio UV−visible spectrometer (Varian) fitted with a temperature controlled cuvette holder utilizing a RC 20 Lauda temperature control module. Buffers were preheated in a hot water bath connected in line with the temperature control module that maintained constant temperature of the cuvette holder. Acetoin substrate kinetics assays were carried out in 100 mM sodium phosphate buffer, pH 6.1. AdhD (1 μL of either 17 μM "free" AdhD or 65.4 μM encapsidated AdhD), both encapsidated (stock concentration) and "free", was added to preheated cuvettes containing acetoin (0.1−100 mM) and NADH (280 μM) in phosphate buffer to give a total reaction volume of 100 μL. This volume was mixed thoroughly by pipeting, and the disappearance of reduced cofactor was monitored by a decrease in absorbance at 340 nm (ε = 6.22 mM^{-1} cm^{-1}). NADH cofactor kinetics assays were carried out similarly, enzyme samples were added to phosphate buffer containing 100 mM acetoin for P22 encapsidated enzyme and 40 mM acetoin for "free" enzyme, and NADH (10−300 μM) with a final volume of 100 μL. The activity assays were carried out in triplicate and performed at 50°, 60°, and 70 °C. Plots of the initial rates of NADH depletion, corrected for nonenzymatic temperature-induced degradation of NADH, were fit to Michaelis−Menten kinetics model using Prism 5 (GraphPad Sofware Inc.) graphing software.

Conflict of Interest: The authors declare no competing financial interest.

Acknowledgment. This work was supported by a grant from the National Science Foundation (BMAT-1104876).

Supporting Information Available: Complete gene and protein sequences for the CP and AdhD-SP, activity assay plots with fits, data comparing the kinetics of "free" enzyme with that of enzyme mixed with P22, multiangle laser light scattering and dynamic light scattering data, and detailed descriptions and an example for the calculations. This material is available free of charge *via* the Internet at http://pubs.acs.org.

REFERENCES AND NOTES

1. Mateo, C.; Palomo, J. M.; Fernandez-Lorente, G.; Guisan, J. M.; Fernandez-Lafuente, R. Improvement of Enzyme Activity, Stability and Selectivity *via* Immobilization Techniques. *Enzyme Microb. Technol.* **2007**, *40*, 1451–1463.
2. Sheldon, R. A. Enzyme Immobilization: The Quest for Optimum Performance. *Adv. Synth. Catal.* **2007**, *349*, 1289–1307.
3. Tran, D. N.; Balkus, K. J. Perspective of Recent Progress in Immobilization of Enzymes. *ACS Catal.* **2011**, *1*, 956–968.
4. van Dongen, S. F. M.; Nallani, M.; Cornelissen, J. L. L. M.; Nolte, R. J. M.; van Hest, J. C. M. A Three-Enzyme Cascade

Reaction through Positional Assembly of Enzymes in a Polymersome Nanoreactor. *Chem.—Eur. J.* **2009**, *15*, 1107–1114.
5. Tanner, P.; Onaca, O.; Balasubramanian, V.; Meier, W.; Palivan, C. G. Enzymatic Cascade Reactions inside Polymeric Nanocontainers: A Means to Combat Oxidative Stress. *Chem.—Eur. J.* **2011**, *17*, 4552–4560.
6. Walde, P.; Ichikawa, S. Enzymes inside Lipid Vesicles: Preparation, Reactivity and Applications. *Biomol. Eng.* **2001**, *18*, 143–177.
7. Vriezema, D. M.; Aragones, M. C.; Elemans, J. A. A. W.; Cornelissen, J. J. L. M.; Rowan, A. E.; Nolte, R. J. M. Self-Assembled Nanoreactors. *Chem. Rev.* **2005**, *105*, 1445–1489.
8. Caruso, F.; Trau, D.; Mohwald, H.; Renneberg, R. Enzyme Encapsulation in Layer-by-Layer Engineered Polymer Multilayer Capsules. *Langmuir* **2000**, *16*, 1485–1488.
9. Minten, I. J.; Claessen, V. I.; Blank, K.; Rowan, A. E.; Nolte, R. J. M.; Cornelissen, J. J. L. M. Catalytic Capsids: The Art of Confinement. *Chem. Sci.* **2011**, *2*, 358–362.
10. Fiedler, J. D.; Brown, S. D.; Lau, J. L.; Finn, M. G. RNA-Directed Packaging of Enzymes within Virus-like Particles. *Angew. Chem., Int. Ed.* **2010**, *49*, 9648–9651.
11. Inoue, T.; Kawano, M. A.; Takahashi, R. U.; Tsukarnoto, H.; Enornoto, T.; Imai, T.; Kataoka, K.; Handa, H. Engineering of SV40-Based Nano-Capsules for Delivery of Heterologous Proteins as Fusions with the Minor Capsid Proteins Vp2/3. *J. Biotechnol.* **2008**, *134*, 181–192.
12. Comellas-Aragones, M.; Engelkamp, H.; Claessen, V. I.; Sommerdijk, N. A. J. M.; Rowan, A. E.; Christianen, P. C. M.; Maan, J. C.; Verduin, B. J. M.; Cornelissen, J. J. L. M.; Nolte, R. J. M. A Virus-Based Single-Enzyme Nanoreactor. *Nat. Nanotechnol.* **2007**, *2*, 635–639.
13. Discher, D. E.; Eisenberg, A. Polymer Vesicles. *Science* **2002**, *297*, 967–973.
14. Uchida, M.; Klem, M. T.; Allen, M.; Suci, P.; Flenniken, M.; Gillitzer, E.; Varpness, Z.; Liepold, L. O.; Young, M.; Douglas, T. Biological Containers: Protein Cages as Multifunctional Nanoplatforms. *Adv. Mater.* **2007**, *19*, 1025–1042.
15. Seebeck, F. P.; Woycechowsky, K. J.; Zhuang, W.; Rabe, J. P.; Hilvert, D. A Simple Tagging System for Protein Encapsulation. *J. Am. Chem. Soc.* **2006**, *128*, 4516–4517.
16. Loo, L.; Guenther, R. H.; Basnayake, V. R.; Lommel, S. A.; Franzen, S. Controlled Encapsidation of Gold Nanoparticles by a Viral Protein Shell. *J. Am. Chem. Soc.* **2006**, *128*, 4502–4503.
17. Loo, L.; Guenther, R. H.; Lommel, S. A.; Franzen, S. Encapsidation of Nanoparticles by Red Clover Necrotic Mosaic Virus. *J. Am. Chem. Soc.* **2007**, *129*, 11111–11117.
18. Chang, C. B.; Knobler, C. M.; Gelbart, W. M.; Mason, T. G. Curvature Dependence of Viral Protein Structures on Encapsidated Nanoemulsion Droplets. *ACS Nano* **2008**, *2*, 281–286.
19. Chen, C.; Daniel, M. C.; Quinkert, Z. T.; De, M.; Stein, B.; Bowman, V. D.; Chipman, P. R.; Rotello, V. M.; Kao, C. C.; Dragnea, B. Nanoparticle-Templated Assembly of Viral Protein Cages. *Nano Lett.* **2006**, *6*, 611–5.
20. Fan, C. G.; Cheng, S. Q.; Liu, Y.; Escobar, C. M.; Crowley, C. S.; Jefferson, R. E.; Yeates, T. O.; Bobik, T. A. Short N-Terminal Sequences Package Proteins into Bacterial Microcompartments. *Proc. Natl. Acad. Sci. U.S.A.* **2010**, *107*, 7509–7514.
21. O'Neil, A.; Reichhardt, C.; Johnson, B.; Prevelige, P. E.; Douglas, T. Genetically Programmed *in Vivo* Packaging of Protein Cargo and Its Controlled Release from Bacteriophage P22. *Angew. Chem., Int. Ed.* **2011**, *50*, 7425–7428.
22. Sun, J.; DuFort, C.; Daniel, M. C.; Murali, A.; Chen, C.; Gopinath, K.; Stein, B.; De, M.; Rotello, V. M.; Holzenburg, A.; *et al.* Core-Controlled Polymorphism in Virus-like Particles. *Proc. Natl. Acad. Sci. U.S.A.* **2007**, *104*, 1354–1359.
23. Worsdorfer, B.; Woycechowsky, K. J.; Hilvert, D. Directed Evolution of a Protein Container. *Science* **2011**, *331*, 589–592.
24. Minten, I. J.; Hendriks, L. J. A.; Nolte, R. J. M.; Cornelissen, J. J. L. M. Controlled Encapsulation of Multiple Proteins in Virus Capsids. *J. Am. Chem. Soc.* **2009**, *131*, 17771–17773.
25. Brasch, M.; de la Escosura, A.; Ma, Y. J.; Uetrecht, C.; Heck, A. J. R.; Torres, T.; Cornelissen, J. J. L. M. Encapsulation of Phthalocyanine Supramolecular Stacks into Virus-like Particles. *J. Am. Chem. Soc.* **2011**, *133*, 6878–6881.
26. Kwak, M.; Minten, I. J.; Anaya, D. M.; Musser, A. J.; Brasch, M.; Nolte, R. J. M.; Mullen, K.; Cornelissen, J. J. L. M.; Herrmann, A. Virus-like Particles Templated by DNA Micelles: A General Method for Loading Virus Nanocarriers. *J. Am. Chem. Soc.* **2010**, *132*, 7834–+.
27. Comellas-Aragones, M.; de la Escosura, A.; Dirks, A. J.; van der Ham, A.; Fuste-Cune, A.; Cornelissen, J. J. L. M.; Nolte, R. J. M. Controlled Integration of Polymers into Viral Capsids. *Biomacromolecules* **2009**, *10*, 3141–3147.
28. de la Escosura, A.; Nolte, R. J. M.; Cornelissen, J. J. L. M. Viruses and Protein Cages as Nanocontainers and Nanoreactors. *J. Mater. Chem.* **2009**, *19*, 2274–2278.
29. de la Escosura, A.; Verwegen, M.; Sikkema, F. D.; Comellas-Aragones, M.; Kirilyuk, A.; Rasing, T.; Nolte, R. J. M.; Cornelissen, J. J. L. M. Viral Capsids as Templates for the Production of Monodisperse Prussian Blue Nanoparticles. *Chem. Commun.* **2008**, 1542–1544.
30. Sikkema, F. D.; Comellas-Aragones, M.; Fokkink, R. G.; Verduin, B. J. M.; Cornelissen, J. J. L. M.; Nolte, R. J. M. Monodisperse Polymer-Virus Hybrid Nanoparticles. *Org. Biomol. Chem.* **2007**, *5*, 54–57.
31. Rhee, J. K.; Hovlid, M.; Fiedler, J. D.; Brown, S. D.; Manzenrieder, F.; Kitagishi, H.; Nycholat, C.; Paulson, J. C.; Finn, M. G. Colorful Virus-like Particles: Fluorescent Protein Packaging by the Q Beta Capsid. *Biomacromolecules* **2011**, *12*, 3977–3981.
32. Lau, J. L.; Baksh, M. M.; Fiedler, J. D.; Brown, S. D.; Kussrow, A.; Bornhop, D. J.; Ordoukhanian, P.; Finn, M. G. Evolution and Protein Packaging of Small-Molecule RNA Aptamers. *ACS Nano* **2011**, *5*, 7722–7729.
33. Manchester, M.; Steinmetz, N. F. Viruses and Nanotechnology. Preface. *Curr Top Microbiol. Immunol.* **2009**, *327*, v–vi.
34. Ren, Y.; Wong, S. M.; Lim, L. Y. Folic Acid-Conjugated Protein Cages of a Plant Virus: A Novel Delivery Platform for Doxorubicin. *Bioconjugate Chem.* **2007**, *18*, 836–843.
35. Ren, Y. P.; Wong, S. M.; Lim, L. Y. *In Vitro*-Reassembled Plant Virus-like Particles for Loading of Polyacids. *J. Gen. Virol.* **2006**, *87*, 2749–2754.
36. Ren, Y. P.; Wong, S. M.; Lim, L. Y. Application of Plant Viruses as Nano Drug Delivery Systems. *Pharm. Res. (Dordrecht, Neth.)* **2010**, *27*, 2509–2513.
37. Wang, T. J.; Zhang, Z. P.; Gao, D.; Li, F.; Wei, H. P.; Liang, X. S.; Cui, Z. Q.; Zhang, X. E. Encapsulation of Gold Nanoparticles by Simian Virus 40 Capsids. *Nanoscale* **2011**, *3*, 4275–4282.
38. Zheng, B.; Zettsu, N.; Fukuta, M.; Uenuma, M.; Hashimoto, T.; Gamo, K.; Uraoka, Y.; Yamashita, I.; Watanabe, H. Versatile Protein-Based Bifunctional Nano-systems (Encapsulation and Directed Assembly): Selective Nanoscale Positioning of Gold Nanoparticle-Viral Protein Hybrids. *Chem. Phys. Lett.* **2011**, *506*, 76–80.
39. Rong, J. H.; Niu, Z. W.; Lee, L. A.; Wang, Q. Self-Assembly of Viral Particles. *Curr. Opin. Colloid Interface Sci.* **2011**, *16*, 441–450.
40. Lee, L. A.; Nguyen, H. G.; Wang, Q. Altering the Landscape of Viruses and Bionanoparticles. *Org. Biomol. Chem.* **2011**, *9*, 6189–6195.
41. Li, K.; Nguyen, H. G.; Lu, X. B.; Wang, Q. Viruses and Their Potential in Bioimaging and Biosensing Applications. *Analyst* **2010**, *135*, 21–27.
42. Lee, L. A.; Niu, Z. W.; Wang, Q. Viruses and Virus-like Protein Assemblies-Chemically Programmable Nanoscale Building Blocks. *Nano Res.* **2009**, *2*, 349–364.
43. Tanaka, S.; Sawaya, M. R.; Yeates, T. O. Structure and Mechanisms of a Protein-Based Organelle in *Escherichia coli*. *Science* **2010**, *327*, 81–84.
44. Kang, S.; Douglas, T. Some Enzymes Just Need a Space of Their Own. *Science* **2010**, *327*, 42–43.
45. Ritsert, K.; Huber, R.; Turk, D.; Ladenstein, R.; Schmidtbase, K.; Bacher, A. Studies on the Lumazine Synthase/Riboflavin Synthase Complex of Bacillus-Subtilis—Crystal-Structure Analysis of Reconstituted, Icosahedral Beta-Subunit Capsids

with Bound Substrate-Analog Inhibitor at 2.4 Angstrom Resolution. *J. Mol. Biol.* **1995**, *253*, 151–167.
46. Tanaka, S.; Kerfeld, C. A.; Sawaya, M. R.; Cai, F.; Heinhorst, S.; Cannon, G. C.; Yeates, T. O. Atomic-Level Models of the Bacterial Carboxysome Shell. *Science* **2008**, *319*, 1083–1086.
47. Sutter, M.; Boehringer, D.; Gutmann, S.; Guenther, S.; Prangishvili, D.; Loessner, M. J.; Stetter, K. O.; Weber-Ban, E.; Ban, N. Structural Basis of Enzyme Encapsulation into a Bacterial Nanocompartment. *Nat. Struct. Mol. Biol.* **2008**, *15*, 939–947.
48. Zhou, Z. H.; McCarthy, D. B.; O'Connor, C. M.; Reed, L. J.; Stoops, J. K. The Remarkable Structural and Functional Organization of the Eukaryotic Pyruvate Dehydrogenase Complexes. *Proc. Natl. Acad. Sci. U.S.A.* **2001**, *98*, 14802–14807.
49. Botstein, D.; Waddell, C. H.; King, J. Mechanism of Head Assembly and DNA Encapsulation in Salmonella Phage-P22. 1. Genes, Proteins, Structures and DNA Maturation. *J. Mol. Biol.* **1973**, *80*, 669–695.
50. Teschke, C. M.; McGough, A.; Thuman-Commike, P. A. Penton Release from P22 Heat-Expanded Capsids Suggests Importance of Stabilizing Penton-Hexon Interactions During Capsid Maturation. *Biophys. J.* **2003**, *84*, 2585–2592.
51. Casjens, S.; Adams, M. B.; Hall, C.; King, J. Assembly-Controlled Autogenous Modulation of Bacteriophage-P22 Scaffolding Protein Gene-Expression. *J. Virol.* **1985**, *53*, 174–179.
52. Parent, K. N.; Khayat, R.; Tu, L. H.; Suhanovsky, M. M.; Cortines, J. R.; Teschke, C. M.; Johnson, J. E.; Baker, T. S. P22 Coat Protein Structures Reveal a Novel Mechanism for Capsid Maturation: Stability without Auxiliary Proteins or Chemical Crosslinks. *Structure* **2010**, *18*, 390–401.
53. Parker, M. H.; Casjens, S.; Prevelige, P. E. Functional Domains of Bacteriophage P22 Scaffolding Protein. *J. Mol. Biol.* **1998**, *281*, 69–79.
54. Weigele, P. R.; Sampson, L.; Winn-Stapley, D.; Casjens, S. R. Molecular Genetics of Bacteriophage P22 Scaffolding Protein's Functional Domains. *J. Mol. Biol.* **2005**, *348*, 831–844.
55. Cheung, C. L.; Camarero, J. A.; Woods, B. W.; Lin, T.; Johnson, J. E.; De Yoreo, J. J. Fabrication of Assembled Virus Nanostructures on Templates of Chemoselective Linkers Formed by Scanning Probe Nanolithography. *J. Am. Chem. Soc.* **2003**, *125*, 6848–6849.
56. Klem, M. T.; Suci, P.; Britt, D. W.; Young, M.; Douglas, T. In-Plane Ordering of a Genetically Engineered Viral Protein Cage. *J. Adhesion* **2009**, *85*, 69–77.
57. Klem, M. T.; Willits, D.; Young, M.; Douglas, T. 2-D Array Formation of Genetically Engineered Viral Cages on Au Surfaces and Imaging by Atomic Force Microscopy. *J. Am. Chem. Soc.* **2003**, *125*, 10806–10807.
58. Steinmetz, N. F.; Calder, G.; Lomonossoff, G. P.; Evans, D. J. Plant Viral Capsids as Nanobuilding Blocks: Construction of Arrays on Solid Supports. *Langmuir* **2006**, *22*, 10032–10037.
59. Machielsen, R.; Uria, A. R.; Kengen, S. W. M.; van der Oost, J. Production and Characterization of a Thermostable Alcohol Dehydrogenase That Belongs to the Aldo-Keto Reductase Superfamily. *Appl. Environ. Microb.* **2006**, *72*, 233–238.
60. Wheeldon, I. R.; Campbell, E.; Banta, S. A Chimeric Fusion Protein Engineered with Disparate Functionalities-Enzymatic Activity and Self-Assembly. *J. Mol. Biol.* **2009**, *392*, 129–142.
61. Brujic, J. Jammed Particles, from Sandy Beaches to Sunscreens. *Phys. Today* **2010**, *63*, 64.
62. Norris, M. G. S.; Malys, N. What Is the True Enzyme Kinetics in the Biological System? An Investigation of Macromolecular Crowding Effect Upon Enzyme Kinetics of Glucose-6-Phosphate Dehydrogenase. *Biochem. Biophys. Res. Commun.* **2011**, *405*, 388–392.
63. Zhou, H. X.; Rivas, G. N.; Minton, A. P. Macromolecular Crowding and Confinement: Biochemical, Biophysical, and Potential Physiological Consequences. *Annu. Rev. Biophys.* **2008**, *37*, 375–397.
64. Olsen, S. N. Applications of Isothermal Titration Calorimetry to Measure Enzyme Kinetics and Activity in Complex Solutions. *Thermochim. Acta* **2006**, *448*, 12–18.
65. Jiang, M.; Guo, Z. H. Effects of Macromolecular Crowding on the Intrinsic Catalytic Efficiency and Structure of Enterobactin-Specific Isochorismate Synthase. *J. Am. Chem. Soc.* **2007**, *129*, 730–731.
66. Cho, Y. K.; Northrop, D. B. Effects of Pressure on the Kinetics of Capture by Yeast Alcohol Dehydrogenase. *Biochemistry* **1999**, *38*, 7470–7475.
67. Northrop, D. B.; Cho, Y. K. Effect of Pressure on Deuterium Isotope Effects of Yeast Alcohol Dehydrogenase: Evidence for Mechanical Models of Catalysis. *Biochemistry* **2000**, *39*, 2406–2412.
68. Park, H.; Girdaukas, G. G.; Northrop, D. B. Effect of Pressure on a Heavy-Atom Isotope Effect of Yeast Alcohol Dehydrogenase. *J. Am. Chem. Soc.* **2006**, *128*, 1868–1872.
69. Kang, S.; Uchida, M.; O'Neil, A.; Li, R.; Prevelige, P. E.; Douglas, T. Implementation of P22 Viral Capsids as Nanoplatforms. *Biomacromolecules* **2010**, *11*, 2804–2809.